

NMR flow velocity mapping in random percolation model objects: Evidence for a power-law dependence of the volume-averaged velocity on the probe-volume radius

H.-P. Müller, R. Kimmich, and J. Weis

Universität Ulm, Sektion Kernresonanzspektroskopie, 89069 Ulm, Germany

(Received 7 June 1996)

Two- or three-dimensional lacunar objects were fabricated using computer-simulated random site-percolation networks as templates. The flow of water pumped through the pore space was studied with the aid of nuclear-magnetic-resonance- (NMR) microscopy modified for mapping of the velocity vector field. The percolation backbones of the objects were determined by exclusion of all pixels or voxels of the spin-density images with velocities below the noise level. An evaluation procedure was established which reliably renders the fractal dimensions of the whole cluster and of its backbone. The volume-averaged velocity magnitude as a function of the probe-volume radius r was found to obey a power law $\bar{v}_V \sim r^{-\lambda}$ in the range $a < r < \xi_v$, where a is the voxel edge length and ξ_v the velocity correlation length. The exponents turned out to be $\lambda = 0.32 \pm 0.04$ and $\lambda = 0.82 \pm 0.03$ for the two- and three-dimensional objects, respectively. In order to test the time dependence of the mean-squared displacement on fractals, $\langle r^2 \rangle = \alpha t^{2/d_w}$, expected for random walks of a fractal dimension d_w , self-diffusion of gaseous methane was examined in the pore spaces of the same objects with the aid of field-gradient NMR diffusometry. The results are in accordance with the theoretical predictions for anomalous diffusion on percolation clusters. This finding is supported by studies of incoherent water flow in the percolation network. [S1063-651X(96)06510-5]

PACS number(s): 47.55.Mh, 87.59.Pw, 47.53.+n, 61.43.Hv

I. INTRODUCTION

Random percolation clusters are subject to characteristic scaling laws with well-defined exponents [1–4]. Parameters of particular interest are the fractal dimension and the correlation length. In our previous work [5,6] we have established a nuclear-magnetic-resonance- (NMR) microscopy procedure permitting the experimental reproduction of analytical or computer-simulated results for random-percolation clusters. The strategy was to use computer-simulated two- or three-dimensional site-percolation clusters as templates for the fabrication of model objects that can be investigated by NMR imaging after filling the pore space with water.

With such a project, several intricacies must be borne in mind. (i) Only a small number of objects can be studied in experiments instead of a real ‘‘ensemble’’ of samples. (ii) The precision of the fabricated objects is limited due to the finite machining resolution. (iii) The spatial resolution in NMR imaging is restricted to a certain minimum voxel size. This is contrasted with the more or less unrestricted ensemble size, and the independence of any spatial resolution of analytical and computer-simulation studies. The reliable analysis of unknown percolation objects (compare [7–10]) in terms of fractal parameters is only permissible after having tested the experimental protocol in a known situation.

In the present study we extend the investigation from purely structural properties to transport phenomena. This, of course, refers to percolation features of utmost practical relevance [11].

Transport parameters of percolation clusters were already the subject of diverse computer simulations as well as dc conductivity measurements [4]. Fluid transport by flow in

such networks tends to be more complicated owing to the influences of capillary pressure, surface tension, and turbulences. The transport limiting structure is the percolation backbone rather than the whole cluster [12]. It is therefore of interest to have experimental means for the determination of the backbone and its structural parameters. That is, ‘‘dangling ends’’ that are not necessary for maintaining the connectivity of the pore network must be identified.

Self-diffusion explored on the length scale of NMR diffusometry may closely be related to the microstructure of the pores [13–15]. However, on a longer scale at which self-diffusion tends to be anomalous as long as the correlation length is not exceeded by the root-mean-squared displacement [16,17], the exponents of the corresponding power laws directly mirror the fractal parameters of the cluster. Therefore it is of interest to check anomalous self-diffusion in lacunar model objects with respect to consistence with fractal parameters on a structural basis.

In the following, fractal parameters and scaling laws determined in computer simulations will be juxtaposed to results derived from NMR-microscopy and field-gradient NMR-diffusometry experiments carried out with model objects of site-percolation networks. The NMR-based examination of water flow and gas diffusion in the rebuilt networks gives direct experimental access to the characteristic transport parameters. The two main objectives are to find answers to the following questions.

(1) Is there any characteristic law for the mean velocity depending on the probe-volume radius?

(2) Does the fractal dimension determined from the mean porosity as a function of the probe-volume radius coincide with that evaluated from anomalous gas diffusion in the pore space?

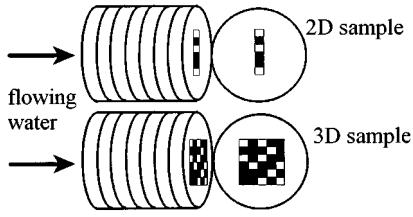


FIG. 1. Schematic illustration of the two- or three-dimensional site-percolation objects used in the experiments. The objects were composed of 32 polystyrene disks of a thickness of 0.5 mm. The pore textures in the disks were machined according to computer-simulated templates. The cross section of the three-dimensional percolation cluster was $16 \times 16 \text{ mm}^2$.

II. EXPERIMENTAL DETAILS

The percolation cluster objects (Fig. 1) were composed of stacks of 0.5 mm thick polystyrene disks which were fabricated according to computer-simulated templates with the aid of a LPKF (Leiterplatten-Konturfäsen) circuit board plotter. The cubic basis of the cluster lattice consisted of 32 lattice constants in each space direction. The cross sections of the pores were quadratic with an edge length of 0.5 mm.

The pore space was investigated after filling it with water (imaging) or methane gas (diffusion). Before injecting water, the pore space was evacuated in order to avoid air bubbles. Magnetic field inhomogeneities in the field of view were less than $\pm 0.015 \text{ ppm}$ as detected by magnetic resonance spectroscopic imaging (e.g., [18]).

Proton magnetic resonance imaging experiments were carried out with a Bruker Biospec 47/40 magnet (4.7 T) combined with a partly homemade radio frequency (rf) unit. The maximum gradients were 0.6 T/m. Typical gradient switching times were 0.2 ms.

Two- or three-dimensional (proton) spin-density image data were recorded using a gradient-recalled echo pulse sequence [Fig. 2(a)]. The digital resolution was 0.25 mm in each spatial dimension. The sample thickness was 16 mm.

Velocity vector maps were acquired using a modification of the Fourier encoding velocity imaging (FEVI) technique [5,19,20]. The pulse scheme is shown in Fig. 2(a). The three components of the local velocity vector were encoded with the aid of bipolar gradient pulses in three successive experiments.

The stimulated-echo variant, Fig. 2(b), was chosen for pulsed field-gradient NMR-diffusometry experiments (e.g., [21]) because we were interested in a particularly wide variation range of the effective diffusion time Δ . For the same reason the field gradients externally applied were kept relatively low (but still about ten times larger than the internal gradients in the percolation objects). Therefore techniques providing strong field gradients such as the supercon fringe field variant [22] were not suitable for our purpose.

Stimulated-echo signals were recorded as a function of the diffusion time Δ in order to gain information on the time dependence of the mean-squared displacements. The signals from the object matrix were subtracted by recording the matrix signals separately with empty objects. The relaxation attenuation factors were eliminated by division of echo signals recorded under identical conditions but different

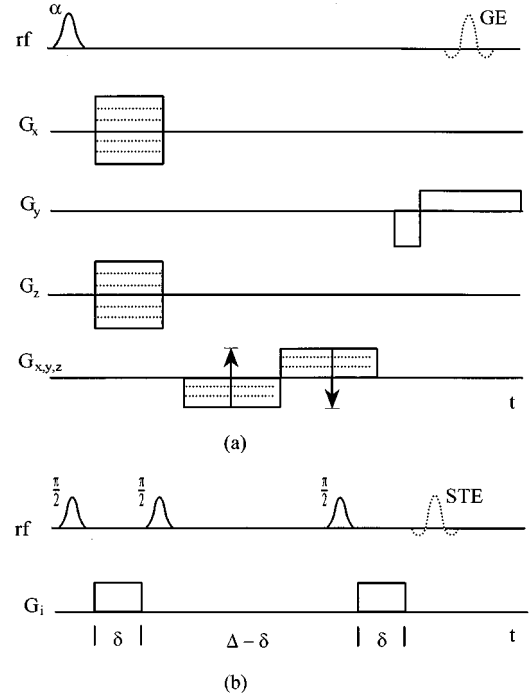


FIG. 2. Radio frequency (rf) and field-gradient (G_i) pulse schemes of the NMR-microscopy and -diffusometry techniques employed in this study. (a) Gradient-recalled echo (GE) pulse sequence for the record of maps of the velocity vector one component after another. The spatial information is acquired by a frequency-encoding gradient in y direction, and phase-encoding gradients along the x and z axes. The latter are incremented independently in subsequent transients. The velocity components are phase encoded by bipolar gradients along the component direction. These gradients are again incremented in subsequent transients independent of the spatial encoding steps. (b) Stimulated-echo (STE) pulse sequence for pulsed field-gradient NMR diffusometry. For the detection of echo attenuations by incoherent flow, the direction of the gradient must be perpendicular to the main-stream direction.

strengths of the gradient pulses (30 mT/m and 12 mT/m). The length of the gradient pulses was $\delta = 0.2 \text{ ms}$.

III. THEORETICAL BACKGROUND AND DEFINITIONS

A. Structural parameters

The scaling window of self-similarity is $a < r < \xi$, where a is the microscopic lattice distance, and ξ the correlation length. Site-percolation clusters in this range have a volume-averaged density varying with the probe-volume radius according to [4]

$$\rho(r) \sim \begin{cases} r^{d_f - d_E}, & a < r < \xi \\ P_\infty, & r > \xi. \end{cases} \quad (1)$$

The Euclidean dimension is denoted by d_E , the fractal dimension by d_f . The percolation probability P_∞ is a constant. Furthermore, the parameters ξ and P_∞ obey [4]

$$P_\infty \sim (p - p_c)^\beta, \quad (2)$$

$$\xi \sim (p - p_c)^{-\nu}, \quad (3)$$

TABLE I. Theoretical parameters of random site percolation clusters [4,17].

d_E	p_c	d_f	β	ν	d_f^b	d_w	μ
2	0.5927	91/48	5/36	4/3	1.6, ..., 1.8	2.6, ..., 2.9	1.3
3	0.3116	2.53	0.41	0.88	1.7, ..., 1.9	3.4, ..., 3.8	2.0

where p is the site occupation probability, and p_c the threshold value of the percolation network. Numerical literature values are listed in Table I. The exponents of the above power laws are related with each other according to [4]

$$d_f = d_E - \frac{\beta}{\nu}. \quad (4)$$

The relations Eqs. (1)–(4) can be verified by computer simulations of site-percolation clusters. The problem arising with real experiments such as those carried out by NMR imaging [5,6] is that the cluster matrix sizes and the ensembles under consideration are relatively small. It was therefore essential to develop evaluation procedures coping with such restrictions. Satisfying solutions are reported in Ref. [5].

In water-filled pore spaces, the water NMR signal is proportional to the water proton spin density, which in turn is a measure of the porosity of the pore space. With spatial resolution one thus obtains the local porosity, $\rho = \rho(\mathbf{r})$, that is, the volume fraction of the water in the voxel under consideration.

The power law given in Eq. (1) can be tested by determining the mean volume-averaged porosity as a function of the radius r of the probe volume. A suitable evaluation method is the so-called ‘‘sandbox’’ method [1,5]:

$$\bar{\rho}_V(r) = \frac{1}{N_p} \sum_{i=1}^{N_p} \frac{1}{N_v} \sum_{j=1}^{N_v} \rho(\mathbf{r}_j) \quad (|\mathbf{r}_i - \mathbf{r}_j| \leq r), \quad (5)$$

where $\rho(\mathbf{r}_j)$ is the porosity in the voxel at the position \mathbf{r}_j . N_v is the number of voxels in the probe volume. The center of the probe volume must be at a position \mathbf{r}_i belonging to the considered cluster. The condition $|\mathbf{r}_i - \mathbf{r}_j| \leq r$ is the consequence of the spherical shape of the probe volume. The expression in Eq. (5) finally refers to the ensemble mean value of N_p probe volumes of equal size.

B. Transport parameters

Coherent or incoherent flow of fluids and self-diffusion in the pore space of percolation clusters is expected to be influenced by the constraints imposed by the geometric confinements. For example, the mean-squared displacement of a random walk on a random percolation cluster is given by

$$\langle r^2 \rangle = \alpha t^{2/d_w}, \quad (6)$$

where d_w is the fractal dimension of the random walk. In the limit of ordinary diffusion, the parameters take the values $\alpha = 2d_E D$ and $d_w = 2$. The quantity D is the unrestricted self-diffusion coefficient. This is contrasted by random walks on fractal objects at which $d_w > 2$ [2,23].

The self-diffusion coefficient and the dc conductivity Σ are related by [17]

$$\Sigma = \frac{en}{k_B T} D \sim (p - p_c)^\mu, \quad (7)$$

where n is the charge carrier number density and e the carrier charge. The Alexander-Orbach conjecture [2]

$$d_w = 2 - d_E + d_f + \frac{\mu}{\nu} \quad (8)$$

linking all fractal exponents mentioned up to now was recently corrected according to [24]

$$\frac{\mu}{\nu} = d_w - d_f. \quad (9)$$

A question not yet solved is how the conductivity parameters can be related to fluid flow under realistic conditions [25,26]. One of the objectives of current research is to link conductivity relations to fractal scaling laws.

The structural background most important in this context is the percolation backbone with the fractal dimension d_f^b (see Table I). This quantity is related to the fractal dimension by

$$\beta_b = \frac{1}{2}(vd_E + 3\beta) - 1, \quad (10)$$

$$d_f^b = d_E - \frac{\beta_b}{\nu}, \quad (11)$$

where β_b is an exponent for the backbone analog to Eq. (2) [27].

In context with the experiments to be presented in the following, we now define the ‘‘mean volume-averaged velocity’’

$$\bar{v}_V(r) = \frac{1}{N_p} \sum_{i=1}^{N_p} \frac{1}{N_v} \sum_{j=1}^{N_v} v(\mathbf{r}_j) \quad (|\mathbf{r}_i - \mathbf{r}_j| \leq r), \quad (12)$$

in analogy to the mean volume-averaged porosity Eq. (5). The local velocity in a voxel at a position \mathbf{r}_j is $v(\mathbf{r}_j) = \sqrt{v_x^2 + v_y^2 + v_z^2}$. The numbers N_v and N_p have the same meaning as in Eq. (5).

IV. COMPUTER SIMULATION OF TWO- AND THREE-DIMENSIONAL PERCOLATION NETWORKS

The percolation objects used for the NMR experiments are based on computer simulations of random site-percolation clusters which served as templates for the object fabrication. The simulations were carried out with the same spatial resolution relative to the object size as the voxel resolution of 0.25 mm operational in the experiments. Each cluster site is covered by four pixels in two-dimensional clusters or eight voxels in three dimensions.

The site-percolation clusters were composed on a cubic lattice with the aid of the random-number generator of the Borland C programming language. Each site of the lattice is occupied randomly with the probability p . The occupation of two neighboring lattice sites is interpreted as a passage. Above the percolation threshold p_c (see Table I) one largest cluster exists connecting opposite edges of the network [see the ‘‘white’’ cluster in Fig. 3(a), for instance]. All isolated

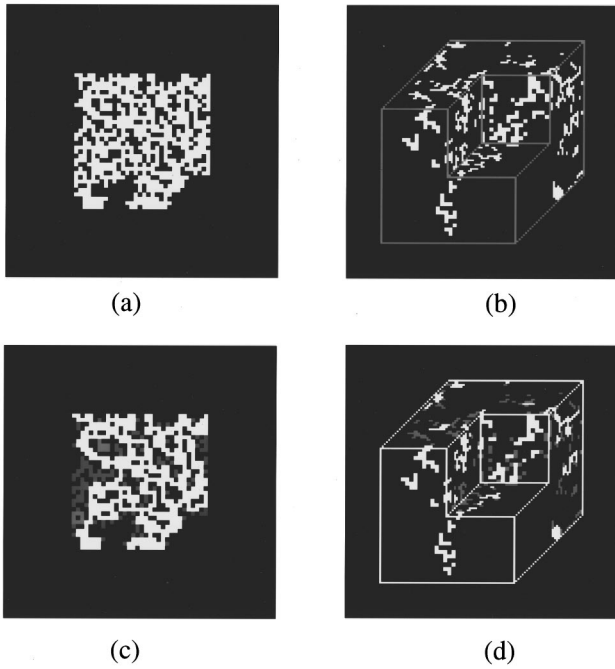


FIG. 3. Computer-simulated site-percolation networks with matrix sizes of 32×32 and $32 \times 32 \times 32$ lattice points in two and three Euclidean dimensions, respectively. Any isolated clusters were eliminated. The white voxels represent the pore space. In the three-dimensional case, the pore voxels are displayed only if they are located on the surface of the multisectional view shown. (a) $d_E=2$, $p-p_c=0.060$. (b) $d_E=3$, $p-p_c=0.035$. (c) $d_E=2$; white voxels: backbone of (a); gray voxels: deadends. (d) $d_E=3$, white voxels: backbone of (b); gray voxels: deadends.

clusters are eliminated [that is, represented as “black” pixels in Figs. 3(a) and 3(b)].

The network size that can be examined in the NMR-microscopy experiments is restricted to $32 \times 32 \times 32$ for practical reasons [5]. Nevertheless the fabricated objects were found to be in complete accordance with the expected fractal properties (see Fig. 4 and Table II). In particular, the scaling laws Eqs. (1)–(4) were verified for all simulated networks used as templates of the fabricated objects [5]. Only patterns without isolated voxel islands were considered, of course.

The definition of the percolation backbone is that there two independent pathways to the sample edges emerge from each site [12]. The corresponding pixels or voxels are displayed in white in Figs. 3(c) and 3(d), whereas the singly connected sites belonging to the deadends are displayed in “gray.” A corresponding computer-based evaluation procedure renders the fractal backbone dimensions listed in Table II. The data fit well to the values expected from the theory for two-dimensional networks (Table I), but differ somewhat from that for three-dimensional clusters. The latter deviation is conceivable because relatively large $p-p_c$ values had to be combined with relatively small matrix sizes for practical reasons.

V. NMR MICROSCOPY AND DIFFUSOMETRY OF FLUIDS AND GASES IN THE PORE SPACE

A. Black-and-white conversion of spin-density images

Figures 4(a) and 4(c) show the spin-density images of static water filled in the pore space of percolation objects

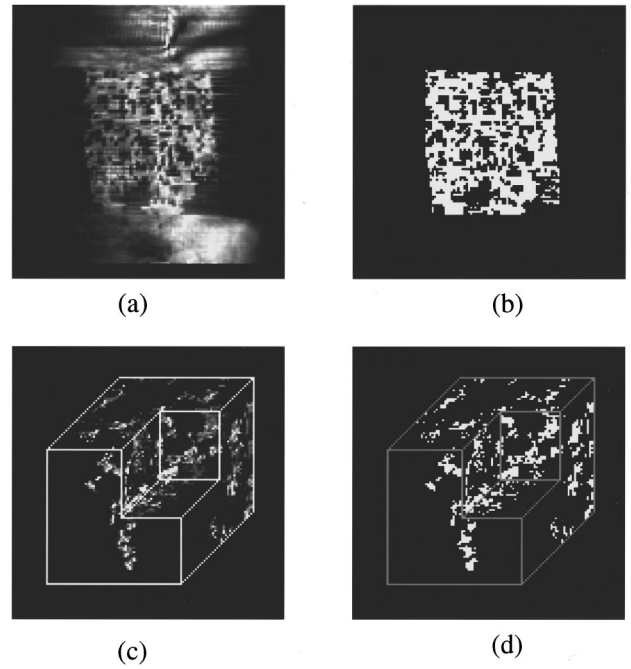


FIG. 4. Spin-density images of the water-filled pore space of two- or three-dimensional percolation objects. In the three-dimensional case, the pore voxels are displayed only if they are located on the surface of the multisectional view shown. The digital resolution was $250 \mu\text{m}$, the field of view 32 mm in each dimension. (a) $d_E=2$, $p-p_c=0.060$ [corresponds to the computer simulation in Fig. 3(a)]. (b) $d_E=2$, black-and-white converted representation of (a). (c) $d_E=3$, $p-p_c=0.035$ [corresponds to the computer simulation in Fig. 3(b)]. (d) $d_E=3$, black-and-white converted representation of (c).

which were fabricated on the basis of the computer-simulated clusters, Figs. 3(a) and 3(b). The gray shades directly reflect the local porosity in the voxels. That is, there are not only “pure” matrix and “pure” pore space voxels as in the case of the computer-simulated clusters. Apart from that, the water signals are unavoidably superimposed by noise in the NMR experiments. On the other hand, the visual inspection reveals a good coincidence of the simulated and the measured patterns in spite of inaccuracies intrinsic to the machining process of the object disks.

The mean volume-averaged porosity [Eq. (5)] for probe-volume radii below the correlation length is only defined for

TABLE II. Fractal dimensions d_f and d_f^b of computer-simulated random site-percolation clusters and their backbones. The cubic site matrix consisted of 32×32 and $32 \times 32 \times 32$ lattice points in two and three Euclidean dimensions, respectively. The statistical errors are ± 0.01 for d_f and ± 0.04 for d_f^b .

p	$d_E=2$		p	$d_E=3$	
	d_f	d_f^b		d_f	d_f^b
0.6527	1.88	1.75	0.3266	2.52	2.15
0.6627	1.90	1.83	0.3466	2.51	2.20
0.6677	1.89	1.79	0.3616	2.55	2.27
0.6727	1.89	1.80	0.3666	2.56	2.28
0.6877	1.89	1.85	0.3816	2.58	2.30

TABLE III. Fractal dimensions d_f and d_f^b evaluated from black-and-white converted and velocity-filtered NMR spin-density images, respectively. The values for d_f^b are averages over several experiments with different flow rates. The statistical errors are ± 0.01 for d_f and ± 0.05 for d_f^b .

p	$d_E=2$		p	$d_E=3$	
	d_f	d_f^b		d_f	d_f^b
0.6527	1.88	1.66	0.3266		
0.6627	1.90	1.74	0.3466	2.53	2.24
0.6677	1.88	1.80	0.3616	2.52	2.31
0.6727	1.87	1.78	0.3666	2.53	2.28
0.6877	1.89	1.81	0.3816		

pixels or voxels belonging either to the pore space or to the matrix. The gray-scale images had therefore to be converted to black-and-white contrasts before any evaluation of mean volume-averaged porosities. A straightforward procedure for this purpose is described in [5].

The fractal dimensions evaluated from the black-and-white converted images are listed in Table III in good coincidence with values directly assessed from the computer simulations (Table II).

B. The percolation backbone

NMR-microscopy experiments were carried out with static water and water flowing through the percolation objects (see Fig. 1). The combination of two- or three-dimensional spin density with velocity maps permits the unambiguous rendering of images of the percolation backbone according to the very definition.

The absolute values of the flow velocity in the voxels, $v = \sqrt{v_x^2 + v_y^2 + v_z^2}$, were calculated from the three velocity components separately measured in the FEVI experiments. The main-flow direction was along the z direction. The histograms of the components and the absolute values of the velocity vectors are shown in Fig. 5 for a two-dimensional percolation network. The velocity noise level was estimated to be 0.8 mm/s for a direction perpendicular to the two-dimensional percolation network used in that experiment.

The black-white converted spin-density images were processed one voxel after another using the velocity magnitude data as criterion for the percolation backbone. Voxels having a water velocity below the rms noise level determined with the histogram, Fig. 5(b), in the flowing-water experiment are excluded from the black-white converted spin-density image and taken as “black.” On the other hand, voxels with higher velocities are considered to belong to the percolation backbone and are left “white.” The resulting percolation backbones are displayed in Figs. 6(b) and 6(d). Varying the flow rate does not significantly change the backbone structure.

The mean volume-averaged porosity of the percolation backbones was evaluated as a function of the probe-volume radius. The results are shown in Figs. 7(a) and 7(b). The values of the backbone fractal dimension are listed in Table III. These data agree well with the values obtained directly from the computer simulations (see Table II).

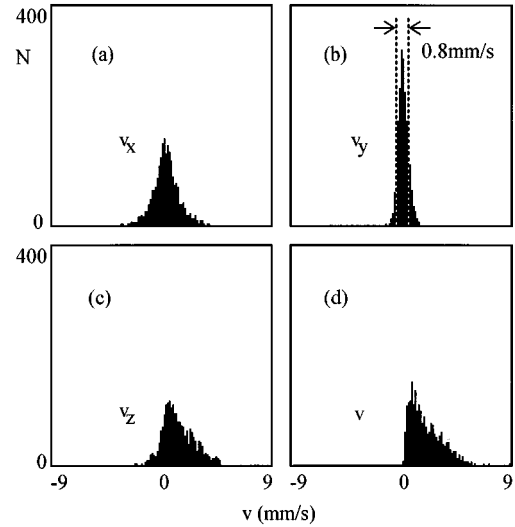


FIG. 5. Histograms of the velocity components and the velocity magnitude of water flowing through the two-dimensional random-percolation object Fig. 4(a) lying in the x/z plane. The main-flow direction was along the z axis. The velocity vector field was recorded using the FEVI method [Fig. 2(a)]. N is the number of voxels in which the respective velocity value was measured. The velocity resolution was 0.14 mm/s. The histogram of the velocity component in the plane of the cluster perpendicular to the main-flow direction, i.e., along the x axis, is symmetrically distributed. In the y direction no real flow is possible. The distribution thus reflects noise with an estimated rms level of 0.8 mm/s.

C. The mean volume-averaged velocity

The mean volume-averaged velocity is defined in Eq. (12). Corresponding evaluations of the velocity (magnitude) maps revealed a certain velocity correlation length ξ_v and a power-law behavior in the radius range below ξ_v (see Fig. 8). The data can be represented by the relation

$$\bar{v}_V(r) \sim \begin{cases} r^{-\lambda}, & a < r < \xi_v \\ \text{const.}, & r > \xi_v \end{cases} \quad (13)$$

which is quite analogous to Eq. (5) for the mean volume-averaged porosity. The exponents λ evaluated from the experimental data are listed in Table IV for different separations $p - p_c$ from the percolation threshold. Average values are $\lambda = 0.32 \pm 0.04$ and $\lambda = 0.82 \pm 0.03$ for two and three Euclidean dimensions, respectively. No obvious correlation between λ and the other fractal parameters, especially the conductivity parameter μ mentioned above, could be stated.

D. Self-diffusion of methane gas confined in the pore space

The root-mean-squared displacement of molecules confined in a fractal pore space is expected to show an anomalous time dependence [Eq. (6)] in the range $a < \sqrt{\langle r^2 \rangle} < \xi$. With the rebuilt three-dimensional percolation objects this range is roughly $0.5 \text{ mm} < \sqrt{\langle r^2 \rangle} < 2 \text{ mm}$.

A crude estimation based on Eq. (6) using $\alpha = 6D$, $D \approx 10^{-9} \text{ m}^2/\text{s}$, $d_w = 2$, and $t \approx \Delta = 10, \dots, 30 \text{ ms}$ readily shows that the detection of the pore-space confinement by field-gradient NMR-diffusometry of fluids is not feasible in

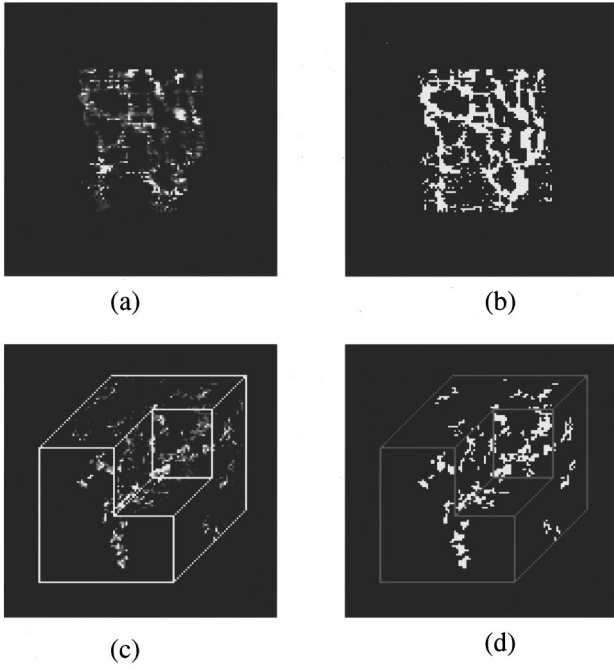


FIG. 6. Velocity maps of water percolating through random site-percolation objects. (a) $d_E=2$, $p-p_c=0.060$ [corresponds to Figs. 3(a) and 4(a)]: The velocity magnitude is represented by gray scales. The intensity is proportional to the absolute value of the velocity $v=(v_x^2+v_y^2+v_z^2)^{1/2}$. (b) $d_E=2$, $p-p_c=0.060$: Percolation backbone, experimentally derived by combining the spin-density data Fig. 4(a) and the velocity map (a). (c) $d_E=3$, $p-p_c=0.035$ [corresponds to Figs. 3(b) and 4(c)]: The velocity magnitude is by gray scales. The intensity is proportional to the absolute value of the velocity $v=(v_x^2+v_y^2+v_z^2)^{1/2}$. (d) $d_E=3$, $p-p_c=0.035$: Percolation backbone, experimentally derived by combining the spin-density data Fig. 4(c) and the velocity map (c).

our case. This is in contrast to diffusion studies on much shorter length scales such as water confined in protein aerogels [28,29].

In the present application, gas diffusion has therefore been studied which provides root-mean-square displacements larger by orders of magnitude than liquid diffusion. As such, we have chosen methane (CH_4), the room temperature bulk self-diffusion coefficient of which is $D=2.0 \times 10^{-5} \text{ m}^2/\text{s}$. The root-mean-squared displacement thus exceeds the

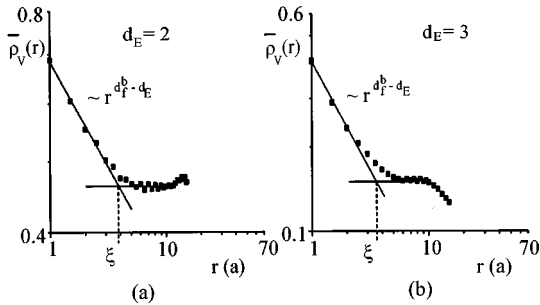


FIG. 7. Mean volume-averaged porosity of percolation backbones. (a) $\bar{\rho}_V(r)$ for the black-and-white converted representation Fig. 6(b). (b) $\bar{\rho}_V(r)$ for the black-and-white converted representation Fig. 6(d).

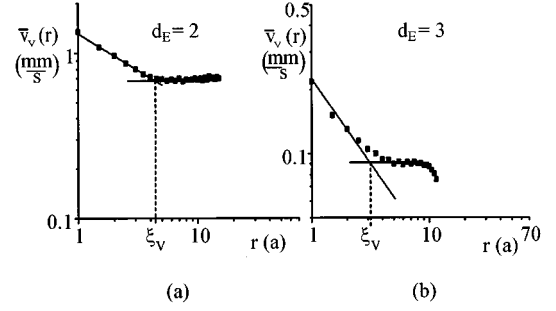


FIG. 8. Mean volume-averaged velocity evaluated from maps of the absolute value of the velocity Figs. 6(a) and 6(c). (a) $d_E=2$, $p=0.6527$. (b) $d_E=3$, $p=0.3466$.

given pore dimensions considerably on the experimental time scale.

The attenuation of the stimulated-echo amplitude by anomalous self-diffusion is expected to follow the relation [21,30]

$$A = A_0 \exp \left[-\gamma G_i \delta^2 \frac{\alpha}{6} \Delta^{2/d_w} \right], \quad (14)$$

where the limit $\delta \ll \Delta$ was assumed [see Fig. 2(b)], and γ is the gyromagnetic ratio.

The self-diffusion behavior of the methane gas was strongly influenced by the pore-space confinement in full accordance with the expectations. Compared with the bulk, the echo attenuation curves of the confined gas were strongly flattened, as demonstrated in Fig. 9. Adopting the theoretically predicted value of $d_w=3.51$ (Table I), the parameter α was fitted to be $(5.0 \pm 1.0) \times 10^{-6} \text{ m}^2/\text{s}^{0.57}$.

E. Incoherent water flow in the pore space

Displacements by flow can be made much larger than those originating from self-diffusion. Flow of a liquid through a percolation network is coherent in the main-stream direction. That is, the velocity vector of a particle is preferentially oriented in that direction during the whole experimental probe time. Coherent displacements lead to phase shifts of the echo signals whereas the echo amplitude is retained.

TABLE IV. Exponents for the power-law dependence of the mean volume-averaged velocity on the probe-volume radius. Different flow rates in the same percolation cluster are of little influence. The data are corresponding averages. The statistical errors are ± 0.02 .

p	$d_E=2$		$d_E=3$		
	$p-p_c$	λ	p	$p-p_c$	λ
0.6527	0.060	0.46	0.3266	0.015	
0.6627	0.070	0.37	0.3466	0.035	0.79
0.6677	0.075	0.26	0.3616	0.050	0.85
0.6727	0.085	0.28	0.3666	0.055	0.82
0.6877	0.095	0.22	0.3816	0.070	

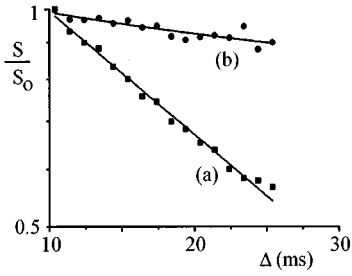


FIG. 9. Stimulated-echo attenuation curves of methane gas at room temperature. (a) Self-diffusion in bulk. The fitted diffusivity is $D = (2.0 \pm 0.5) \times 10^{-5} \text{ m}^2/\text{s}$. (b) Self-diffusion in a rebuilt percolation network. The fitted parameter is $\alpha = (5.0 \pm 1.0) \times 10^{-6} \text{ m}^2/\text{s}^{0.57}$.

This is in contrast to incoherent flow which arises in pore spaces in directions perpendicular to the main-stream direction as was already demonstrated in experiments with water flowing through a natural sponge or densely coiled cotton fibers [28,31]. Experimentally the incoherence reveals itself by an attenuation of the echo amplitude rather than by phase shifts.

The incoherent nature is a matter of the time scale in which the displacements are probed, of course [31]. The velocity components perpendicular to the main stream change their signs according to the microstructure of the pore space. If such sign changes occur frequently on the experimental time scale, the prerequisites of a random walk are given. This sort of motion can therefore be studied using the pulse sequence in Fig. 2(b) at which the field gradient must be directed perpendicular to the main stream. The evaluation formula Eq. (14) for an anomalous displacement behavior is again applicable after redefining the parameters α and d_w for the incoherent-flow case [28].

The stimulated-echo attenuation curves for incoherent water flow through a random-percolation object are shown in Fig. 10. The curve parameter is the average main-flow velocity, which is called Dupuit-Forcheimer velocity v_{DF} . It can be calculated from the total volume flow rate $\langle f \rangle$ via

$$v_{DF} = \frac{\langle f \rangle}{\rho_0 A}, \quad (15)$$

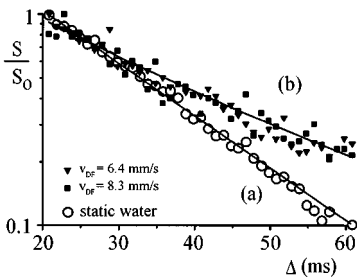


FIG. 10. Stimulated-echo attenuation curves of water at room temperature. (a) Static water [$d_w = 2$, $D = (2.0 \pm 0.5) \times 10^{-9} \text{ m}^2/\text{s}$]. (b) Water incoherently percolating through a rebuilt three-dimensional percolation object. The (diffusion) gradient direction was chosen perpendicular to the main-flow direction. The fitted parameters are $d_w = 2.60 \pm 0.04$, $\alpha = (2.0 \pm 0.3) \times 10^{-9} \text{ m}^2/\text{s}$. The Dupuit-Forcheimer velocity was varied from 6.4 mm/s to 8.3 mm/s.

where A is the total percolated area and ρ_0 the average porosity of the sample [9]. Without flow the attenuation is solely due to self-diffusion. The additional displacements caused by incoherent flow are obvious. The nonexponentiality of the decays indicates incoherent displacements similar to those due to anomalous self-diffusion.

The fractal dimension of the random walk caused by the incoherent motions was fitted to be $d_w = 2.60 \pm 0.04$. This value deviates from that expected for self-diffusion on a random percolation cluster (see Table I). The reason is attributed to contributions by self-diffusion in static water in the deadends. For the parameter α we obtained $(1.9 \pm 0.3) \text{ m}^2/\text{s}^{0.77}$.

The data do not show any systematic dependence on the flow rate. This finding is interpreted as a structural limit. The displacements by incoherent displacements are mainly determined by the pore-space confinements. In the flow rate range of our experiments the main-stream flow velocity therefore is of minor importance.

VI. CONCLUSIONS AND DISCUSSION

Two- and three-dimensional random percolation clusters were computer simulated. The resulting structures were used as templates for the fabrication of corresponding lacunar objects. The fractal properties of these objects were studied by NMR microscopy and diffusometry after filling the pore spaces with water or methane gas.

The theoretically predicted fractal parameters were juxtaposed to those evaluated from the computer-simulated structures and those assessed with the aid of the NMR experiments with the rebuilt lacunar objects. The percolation backbone was experimentally separated with the aid of a procedure mapping the flow velocity. The percolation backbone is the structure crucial for the transport properties of the cluster [11]. The numerical and experimental results for the fractal dimension and other percolation parameters are in accordance with the theoretical predictions.

Using velocity mapping, the distribution of flow velocities in the lacunar objects was studied. A hitherto unknown power law of the mean volume-averaged velocity as a function of the probe-volume radius was discovered.

Gas diffusion in the percolation objects showed clear indications of the anomalous behavior expected on theoretical grounds. Nevertheless these experiments were somewhat hampered by the low detection sensitivity of methane. Future experiments using ^{129}Xe as probe particles that can be pumped optically [32] are in preparation. It should then be possible to cover a much wider diffusion time range as needed for the unambiguous evaluation of the fractal dimension applying for the random walk, d_w .

Anomalous root-mean-squared displacements were also concluded from incoherent water flow in analogy to our previous studies on flow through natural sponge and coiled cotton fibers [28,31]. It appears that the structure of the percolation cluster forms the factor limiting the local transport perpendicular to the main-stream direction, whereas the total flow rate shows little influence.

ACKNOWLEDGMENTS

We thank Hans Wiringer and Ute Goerke for assistance in the course of the experiments. Financial support by the Alexander von Humboldt Foundation and the Deutsche

Forschungsgemeinschaft is gratefully acknowledged. J.W. is indebted to the Institute of Measurement Science, Slovak Academy of Sciences, Bratislava for continuous support.

-
- [1] *Fractals in Science*, edited by A. Bunde and S. Havlin (Springer-Verlag, Berlin, 1994).
- [2] R. Orbach, *Science* **231**, 814 (1986).
- [3] A. Kapitulnik, A. Aharony, G. Deutscher, and D. Stauffer, *J. Phys. A* **16**, L269 (1983).
- [4] D. Stauffer and A. Aharony, *Introduction to Percolation Theory* (Taylor and Francis, London, 1985).
- [5] H.-P. Müller, J. Weis, and R. Kimmich, *Phys. Rev. E* **52**, 5195 (1995).
- [6] H.-P. Müller, R. Kimmich, and J. Weis, *Magn. Reson. Imaging* (to be published).
- [7] S. N. Sarkar, J. J. Dechter, and R. A. Komoroski, *J. Magn. Reson. A* **102**, 314 (1993).
- [8] D. N. Guilfoyle, P. Mansfield, and K. J. Packer, *J. Magn. Reson.* **97**, 342 (1992).
- [9] G. J. Nesbitt, T. W. Fens, J. S. van den Brink, and N. Roberts, in *Magnetic Resonance Microscopy*, edited by B. Blümich and W. Kuhn (VCH Verlagsgesellschaft mbH, Weinheim, 1992).
- [10] M. R. Merrill, *Bull. Magn. Reson.* **15**, 154 (1993).
- [11] M. Sahimi, *Flow and Transport in Porous Media and Fractured Rock* (VCH Verlagsgesellschaft mbH, Weinheim, 1995).
- [12] J. Mastorakos and P. Argyrakis, *Phys. Rev. E* **48**, 4847 (1993).
- [13] A. Coy and P. T. Callaghan, *J. Colloid Interface Sci.* **168**, 373 (1994).
- [14] A. Coy and P. T. Callaghan, *J. Chem. Phys.* **101**, 4599 (1994).
- [15] P. T. Callaghan, *J. Magn. Reson. A* **113**, 53 (1995).
- [16] *Fractals and Disordered Systems* edited by A. Bunde and S. Havlin (Springer-Verlag, Berlin, 1991).
- [17] S. Havlin and D. Ben-Avraham, *Adv. Phys.* **36**, 695 (1987).
- [18] J. Weis, J. Frollo, and L. Budinski, *Z. Naturforsch, Teil A* **44**, 1151 (1989).
- [19] T. W. Redpath, D. G. Morris, R. A. Jones, and J. M. S. Hutchison, *Phys. Med. Biol.* **29**, 891 (1984).
- [20] J. Bittoun, E. Bourroul, O. Jolivet, I. Idy-Peretti, E. Mousseaux, A. Tardivon, and P. Peronneau, *Magn. Reson. Med.* **29**, 674 (1990).
- [21] J. Kärgler, H. Pfeiffer, and G. Vojta, *Phys. Rev. A* **37**, 4514 (1988).
- [22] R. Kimmich, W. Unrath, G. Schnur, and E. Rommel, *J. Magn. Reson.* **91**, 136 (1991).
- [23] R. Metzler, W. G. Glöckle, and T. F. Nonnenmacher, *Physica A* **211**, 13 (1994).
- [24] D. C. Hong, S. Havlin, H. J. Herrmann, and H. E. Stanley, *Phys. Rev. B* **30**, 4083 (1984).
- [25] P. M. Adler, *Int. J. Multiphase Flow* **11**, 91 (1985).
- [26] I. B. Halperin, S. Feng, and P. N. Sen, *Phys. Rev. Lett.* **54**, 2391 (1985).
- [27] C. Liem and N. Jan, *J. Phys. A* **21**, L243 (1988).
- [28] F. Klammler and R. Kimmich, *Croat. Chem. Acta* **65**, 455 (1992).
- [29] R. Kimmich, F. Klammler, V. D. Skirda, I. A. Serebrennikova, A. I. Maklakov, and N. Fatkullin, *Appl. Magn. Reson.* **4**, 425 (1993).
- [30] G. Jug, *Chem. Phys. Lett.* **131**, 94 (1986).
- [31] F. Klammler and R. Kimmich, *Phys. Med. Biol.* **35**, 67 (1990).
- [32] Y. Q. Song, H. C. Gaede, T. Pietrass, G. A. Barrall, G. C. Chingas, M. R. Ayers, and A. Pines, *J. Magn. Reson. A* **115**, 127 (1995).